

# Discrete transverse superconducting modes in nano-cylinders

J. E. Han and Vincent H. Crespi

*Department of Physics and Materials Research Institute,  
The Pennsylvania State University, University Park, PA 16802-6300*

(Dated: September 22, 2018)

Spatial variation in the superconducting order parameter becomes significant when the system is confined at dimensions well below the typical superconducting coherence length. Motivated by recent experimental success in growing single-crystal metallic nanorods, we study quantum confinement effects on superconductivity in a cylindrical nanowire in the clean limit. For large diameters, where the transverse level spacing is smaller than superconducting order parameter, the usual approximations of Ginzburg-Landau theory are recovered. However, under external magnetic field the order parameter develops a spatial variation much stronger than that predicted by Ginzburg-Landau theory, and gapless superconductivity is obtained above a certain field strength. At small diameters, the discrete nature of the transverse modes produces significant spatial variations in the order parameter with increased average magnitude and multiple shoulders in the magnetic response.

PACS numbers: 74.78.-w, 85.25.-j

## I. INTRODUCTION

Recent developments in nanofabrication techniques allow access to new physical regimes where various intrinsic order parameters interact with a tuneable confining environment. Such order parameters cover an array of diverse physical systems, such as ferromagnets<sup>1</sup>, quantum dots<sup>2</sup>, molecular electronics<sup>3</sup>, photonic crystals<sup>4</sup>, superconductors<sup>5,6,7</sup> etc. Quantum-confined superconductivity is particularly interesting for its macroscopic quantum nature; its well-understood microscopic mechanism can also serve as a platform for studies of other many-body nanoscopic quantum confinement effects.

Since the advent of BCS theory, a great deal has been understood in both the microscopic and phenomenological aspects of superconductivity for conventional phonon-mediated pairing systems. Theories have been immediately applied with great success to small superconductors<sup>7,8</sup> of various geometry<sup>9,10</sup>. Particularly useful has been the phenomenological Ginzburg-Landau theory, which describes superconductivity directly in terms of the superconducting order parameters without appealing to an underlying electronic basis.

Partly due to its enormous success, however, the Ginzburg-Landau theory has sometimes been applied beyond its strict regime of validity, especially in systems of small size. Part of the justification for this has been that experimental samples have often been disordered or polycrystalline, in which case confinement effects are less pronounced than they are for single crystals. Well-established dirty-limit theories for small superconductors with strong disorder<sup>11</sup> describe fascinating physics, such as gapless superconductivity, down to nanometer scales. In the clean limit of microscopic BCS theory, where the mean free path  $\ell$  is longer than the coherence length  $\xi_0$  ( $\ell \gg \xi_0$ ), the superconducting behavior of small samples is very different from that in the dirty limit ( $\ell \ll \xi_0$ )<sup>10,12</sup>. Recent experimental techniques for producing high quality *single crystalline* nanostructures

through electrodeposition into extended nanopores<sup>13</sup> demands a re-examination of the phenomenology of superconductivity in such systems, working from microscopic theories. We specifically aim to investigate the often-overlooked spatial structures of the superconducting order parameter in the confined direction by directly solving the Bogoliubov-de Gennes equation and comparing with other theories.

For the last few decades, work on one-dimensional superconductivity has mostly focused on fluctuation effects<sup>14,15</sup>. These treatments assume featureless transverse superconducting modes within superconducting nanowires and instead concentrate on the physics of phase slips in the *axial* direction. Here we complement these previous approaches by considering the effects of *transverse* quantum confinement on the spatial variation of superconducting order parameter, with consequences for the quasi-particle excitation spectrum and the magnetic response.

## II. FORMALISM

We consider a superconducting cylinder with a radius  $R$  smaller than the penetration depth  $\lambda$ , but much larger than the atomic scale, so that we can describe the system with a continuum basis. The Bogoliubov-de Gennes (BdG) equations are

$$\begin{bmatrix} H_0 & \Delta \\ \Delta^* & -H_0^* \end{bmatrix} \begin{bmatrix} u \\ v \end{bmatrix} = E \begin{bmatrix} u \\ v \end{bmatrix} \quad (1)$$

where  $\Delta$  is the order parameter and  $H_0$  is the Hamiltonian for electrons,

$$H_0 = \frac{1}{2m^*} \left( -i\hbar\nabla - \frac{e}{c}\mathbf{A} \right)^2 - \mu - \mu_B \boldsymbol{\sigma} \cdot \mathbf{H}. \quad (2)$$

Here  $m^*$  is the band electron mass,  $\mu$  is the chemical potential,  $\mu_B$  is the Bohr magneton,  $\boldsymbol{\sigma}$  is the Pauli spin

matrix and  $\mathbf{H}$  is the external magnetic field.  $H_0$  and its complex conjugate  $H_0^*$  act on the time-reversed electrons in Cooper pairs. The state  $[u, v]$  represents the amplitudes of the pair of electrons which interact with each other via the pairing interaction parametrized by the superconducting order parameter  $\Delta$ . For an axial magnetic field,  $\mathbf{H} = H\hat{\mathbf{z}}$ , the vector potential in the Coulomb gauge is:

$$\mathbf{A} = \frac{1}{2}rH\hat{\theta}, \quad (3)$$

where  $\hat{\theta}$  is an unit vector along the azimuthal direction. We assume that the radius of the nanorod is sufficiently below the penetration depth  $\lambda$  that screening of the magnetic field due to demagnetization is negligible. In a cylindrical coordinate system  $H_0$  becomes<sup>16</sup>:

$$H_0 = -\frac{\hbar^2}{2m^*} \left( \frac{\partial^2}{\partial r^2} + \frac{1}{r} \frac{\partial}{\partial r} + \frac{1}{r^2} \frac{\partial^2}{\partial \theta^2} + \frac{\partial^2}{\partial z^2} \right) + \frac{1}{2}i\hbar\omega_c \frac{\partial}{\partial \theta} + \frac{1}{8}m^*\omega_c^2 r^2 - \mu - \mu_B \sigma_z H \quad (4)$$

$$= K^0 + \frac{1}{2}(i\frac{\partial}{\partial \theta} - \sigma_z)\hbar\omega_c + \frac{1}{8}m^*\omega_c^2 r^2, \quad (5)$$

where  $K^0$  is the kinetic energy in zero external field (absorbing the chemical potential) and  $\omega_c = eH/m^*c$  is the cyclotron frequency. With the typical separation of variables, the electron pair for the basis in Eq. (1) consists of time-reversed electrons in states  $(mjk \uparrow)$  and  $(-mj-k \downarrow)$  with  $m$  the azimuthal quantum number in  $e^{im\theta}$  and  $k$  the  $z$ -wavevector in  $e^{ikz}$ . We explicitly write down the BdG equations by expanding  $u(\mathbf{r})$  and  $v(\mathbf{r})$  in terms of the eigenfunctions of  $K^0$  as

$$u_{mj}^k(\mathbf{r}) = u_{mj}^k \phi_{mj}(r) \frac{e^{im\theta}}{\sqrt{2\pi}} \frac{e^{ikz}}{\sqrt{L}} \quad (6)$$

$$v_{mj}^k(\mathbf{r}) = v_{mj}^k \phi_{mj}(r) \frac{e^{im\theta}}{\sqrt{2\pi}} \frac{e^{ikz}}{\sqrt{L}}, \quad (7)$$

with  $L$  the length of the cylinder. We apply a boundary condition

$$u(\mathbf{r}) = v(\mathbf{r}) = 0 \text{ with } |\mathbf{r}| = R, \quad (8)$$

so that the wavefunction vanishes outside the cylinder. This relation only imposes the condition that there are no electrons outside the cylinder and does not make any assumptions on the coarse-grained superconducting order parameters as usually treated in Ginzburg-Landau theory<sup>8</sup>. The radial term

$$\phi_{mj}(r) = \frac{\sqrt{2}}{R J_{m+1}(\alpha_{mj})} J_m \left( \frac{\alpha_{mj} r}{R} \right), \quad (9)$$

where  $J_m$  is the  $m$ -th order Bessel function and  $\alpha_{mj}$  is its  $j$ -th zero. The operator  $K^0$  is diagonal with matrix elements  $K_{mjk}^0 = \hbar^2/2m^*(\alpha_{mj}^2/R^2 + k^2)$ . The BdG equation requires evaluation of matrix elements for  $\langle r^2 \rangle$  and

$\Delta(\mathbf{r})$ . We will consider only the case of order parameters with zero net angular momentum and zero net momentum along  $z$ -axis, namely  $m + m' = 0$  and  $k + k' = 0$  in the product  $u_{mj}^k v_{m'j'}^{k'}$  for order parameter  $\Delta(\mathbf{r})$ . A paired state with finite net (angular) momentum has higher kinetic energy than the stationary solution, and is therefore disfavored<sup>17</sup>. With this choice of order parameter, we can compute the matrix elements for  $\Delta(\mathbf{r})$  and  $r^2$  as

$$\Delta_{m;jj'} = \int_0^R \phi_{mj}(r) \Delta(r) \phi_{mj'}(r) r dr, \quad (10)$$

$$r_{m;jj'}^2 = \int_0^R \phi_{mj}(r) r^2 \phi_{mj'}(r) r dr. \quad (11)$$

The transverse modes (indexed with  $mj$ ) are decoupled from the longitudinal modes (indexed with  $k$ ) and the gap equation is simplified.

The BdG equations Eq. (1) now become (with  $I_{m;jj'} \equiv \frac{1}{2}m^*r_{m;jj'}^2$ ):

$$\left[ K_{mjk}^0 - \frac{1}{2}(m+1)\hbar\omega_c \right] u_{mj}^k + \sum_{j'} \left[ \frac{1}{4}\omega_c^2 I_{m;jj'} u_{mj'}^k + \Delta_{m;jj'} v_{mj'}^k \right] = E_{mj}^k u_{mj}^k \quad (12)$$

$$\left[ -K_{mjk}^0 - \frac{1}{2}(m+1)\hbar\omega_c \right] v_{mj}^k + \sum_{j'} \left[ \frac{1}{4}\omega_c^2 I_{m;jj'} v_{mj'}^k + \Delta_{m;jj'} u_{mj'}^k \right] = E_{mj}^k v_{mj}^k \quad (13)$$

Note that the Zeeman terms  $\frac{1}{2}(m+1)\hbar\omega_c$  have the same sign for  $u_{mj}^k$  and  $v_{mj}^k$  since they represent the amplitudes for time-reversed states. The order parameter  $\Delta(\mathbf{r})$  is self-consistently expressed by the typical gap equation

$$\Delta(\mathbf{r}) = V \sum_{mjk} [1 - 2f(E_{mj}^k)] u_{mj}^k(\mathbf{r}) v_{mj}^k(\mathbf{r})^*, \quad (14)$$

where the summation range for the eigenstates is over kinetic energies  $K_{mjk}^0$  within a window  $[-\omega_D, \omega_D]$  of width twice the Debye frequency  $\omega_D$ . We use generic parameter values suitable for conventional superconductors with  $T_c$  at few Kelvins.  $\Delta$  at  $T = 0$  converges at large diameters as will be shown and we use the converged value  $\Delta_0 = 3.9$  K as the bulk limit throughout this paper.  $m^*$  is set to the free electron mass,  $\omega_D = 100$  K and  $\mu = 10000$  K. As shown below, The Fermi velocity is then  $v_F = 0.55 \times 10^8$  cm/sec and the coherence length  $\xi_0 = \hbar v_F / \pi \Delta_0 \sim 350$  nm in the bulk. Results are plotted in dimensionless units in this paper. Although we have chosen a particular set of parameters, we expect that our conclusion will hold qualitatively for conventional low- $T_c$  superconductors.

As the diameter  $D$  ( $\equiv 2R$ ) shrinks, the transverse kinetic energy becomes very sensitive to the boundary condition, Eq. (8). Defining a variation of radius  $\delta R$ ,  $\delta K^0/K^0 = -2\delta R/R$ . With a small uncertainty in radius  $\delta R = 1$  Å around  $R = 10$  nm, for example,

$\delta K^0 \sim 0.02\mu \sim 200$  K, which is comparable to the Debye frequency. We incorporate the effects of variations in the wire diameter as a noise in the kinetic energy:

$$K_{mjk} = K_{mjk}^0 + s_{mjk} \left| \frac{dK^0}{dR} \right| \delta R, \quad (15)$$

where  $s_{mjk}$  is a random number uniformly distributed in  $[-1, 1]$  and we set  $\delta R \lesssim 5$  Å. Due to the time reversal symmetry of static scattering at the boundary,  $s_{mjk} = s_{-m-j-k}$ . Here, we have partly taken into account the radial variations via energy levels, leaving unchanged the basis functions and the boundary condition. We have sampled equi-spaced  $z$ -momenta in the half Brillouine zone  $[0, \pi]$  with 200 – 500 points, depending on the level of convergence required. Note that experimental nanowire samples to date have a significant variation in diameter along their length, but this variation is often slow on the length-scale of the nanowire width; the longest-wavelength variations could be subsumed into an adiabatic treatment.

### III. RESULTS

The density of states of a nanorod can be expressed as the sum of one-dimensional densities of states  $N_1(E)$  displaced by transverse energy eigenvalues  $E_\alpha$ ,

$$N(E) = \sum_\alpha N_1(E - E_\alpha). \quad (16)$$

Quantized transverse levels strongly affect the density of states. Transverse modes are spaced with an average level spacing  $\delta E = 1/N_2$  with  $N_2$  the 2-dimensional density of states,  $N_2 = (\pi R^2)(m^*/\pi\hbar^2)$ . Since  $N_2$  is independent of the chemical potential, the qualitative results do not depend on the particular position of the chemical potential. More details will be discussed in subsection III B. However,  $N_1(E - E_\alpha)$  has a van Hove singularity at  $E = E_\alpha$  and therefore small changes in the chemical potential can produce quantitatively different results. Confinement effects become strong when the level spacing  $\delta E$  is comparable to  $\Delta$ , *i.e.*,

$$R \lesssim \sqrt{\frac{\hbar^2}{m^* \Delta}}. \quad (17)$$

This condition becomes  $D/\xi_0 \lesssim 0.1$  with our parameters (and  $\Delta = 3.8$  K). Due to the singularities in  $N(E)$ , solutions of the BdG equation are quite sensitive to model parameters for  $D/\xi_0 \lesssim 0.1$ , even including a moderate smearing from  $\delta R$ .

#### A. Large diameters

Superconductivity under confinement has been well studied for samples in the limit of  $\delta E \ll \Delta$  and  $D \ll$

$\lambda^{7,12,18}$ . For cylindrical samples with specular boundary conditions, we can explicitly solve Eq. (14) in the clean limit as a function of external magnetic field along the axis,

$$\begin{aligned} \ln(\Delta/\Delta_0) &= - \left( 1 + \frac{1}{2\alpha^2} \right) \ln \left[ \alpha + \sqrt{\alpha^2 - 1} \right] \\ &\quad + \frac{3}{2} \sqrt{1 - \alpha^{-2}}, \text{ for } \alpha > 1 \\ &= 0, \text{ for } \alpha < 1 \end{aligned} \quad (18)$$

where  $\alpha = h/\Delta$ ,  $h = ev_F RH/2c$ , and  $\Delta_0$  is the order parameter in bulk without external field. Strässler and Wyder<sup>12</sup> have obtained a result similar to the above equation for spherical systems and we follow essentially the same derivation for cylindrical systems in Appendix A. In this solution, we make a major assumption by ignoring the spatial variation of the order parameter, *i.e.*  $\Delta(\mathbf{r}) = \Delta$ . In carrying out an analytic calculation from Eq. (14), we make further approximations that the position and momentum in Eq. (14) commute and that the terms quadratic in the field  $\frac{1}{4}m^*\omega_c^2 I_{mjk}$  in Eq. (13) are negligible. When compared with a numerical solution of the full BdG equations, the above approximations seem reasonable in the large  $D$  regime for zero external magnetic field, (until  $D/\xi_0 \lesssim 0.57$  for our parameter values).

This clean-limit solution has a field dependence quite different from the standard Ginzburg-Landau prediction. Instead of gradually decaying from the zero-field order parameter  $\Delta_0$  to zero,  $\Delta$  stays constant up to  $H_1 = 2c\Delta_0/ev_F R$  and then drops to zero at the critical field  $H_c$ , (see solid line in Fig. 1)

$$H_c = \frac{1}{2} \exp(3/2) H_1 = 0.454 \frac{\Phi_0}{\xi_0 R}, \quad (19)$$

with the flux quantum  $\Phi_0 = hc/2e$  and the coherence length  $\xi_0 = h v_F / \pi \Delta_0$ . The critical field depends inversely on the diameter, since orbital motions of electron in small samples are less influenced by magnetic field.  $H_\xi$  in Fig. 1 is defined as  $H_1$  for  $R = \xi_0$ , *i.e.*,  $H_\xi = 2c\Delta_0/ev_F \xi_0$ .

We have solved the BdG equations under two different conditions: first with the constraint of a spatially uniform order parameter and then with the constraint relaxed. The quantitative results and their overall line shapes (in Fig. 1) are in good agreement with the analytic formula Eq. (18). First comparing the analytic result with the uniform- $\Delta$  calculation, we find that the invariant order parameter up to  $H = H_1$  is well reproduced. The numerical  $\Delta$  deviates downward from the analytical formula at higher values of  $H$ , resulting in smaller critical field  $H_c$ . We attribute the discrepancy to underestimation of the external field in the analytic solution due to ignoring the  $\mathbf{A}^2$  term. Further discussion is given at the end of this subsection.

An important qualitative deviation of the full BdG solution from the uniform- $\Delta$  results comes at high fields near  $H_c$ . The critical field for the full BdG solution (solid

circles in Fig. 1) extends to high fields, with  $\Delta$  decaying much slower than the usual square-root drop<sup>19</sup> of the uniform- $\Delta$  solution. It is clear that this phenomenon must originate from the transverse spatial variation of the order parameter, which we will discuss below in more detail.

Although the average order parameter remains constant for  $0 < H < H_1$  (left to the dashed line in Fig. 1), the density of states reveals a closing of the excitation gap at the field  $H_1$  (dashed curve in Fig. 2), where the spectral weight at the chemical potential becomes finite. The density of states in the gapped region continues to increase until  $H = H_c$ . In the clean limit, the electron trajectories are not perturbed by impurity scattering and their angular momentum  $\mathbf{L}$  couples to the external field as  $-(e/2m^*c)\mathbf{L} \cdot \mathbf{H}$ . This coupling gives the term  $-\frac{1}{2}m\hbar\omega_c$  in Eq. (13) and contributes to the quasi-particle excitation energy  $E_{mj}^k$ ,

$$E_{mj}^k = \sqrt{K_{mj}^0{}^2 + \Delta^2} + \frac{1}{2}(m+1)\hbar\omega_c. \quad (20)$$

These angular momentum contributions dominate over spin contributions and the excitation spectrum goes gapless when  $\Delta \sim (e/2m^*c)\langle \mathbf{L} \cdot \mathbf{H} \rangle \sim ev_F RH/2c$ . In contrast, when impurity scattering dominates, the electron trajectories are disrupted and the quasi-particle energy is no longer in the form of Eq. (20). In this limit, the quasi-particle energy suffers significant level broadening and experiences shifts only from the spin Zeeman terms<sup>20</sup>. Therefore, away from the clean limit the density of states retains the form of a conventional gapped superconductor<sup>12</sup>.

At zero field, the order parameter is nearly constant over the cylinder (see Fig. 3), except for small oscillations and a Gibb's phenomenon at  $r = R$ . The rapid oscillations have a wavelength proportional to  $1/v_F$  and an amplitude that diminishes for larger diameters. Therefore we expect that these oscillations will be averaged out on larger length scales; they are not important for large-diameter systems. In such regime, we correctly reproduce the boundary condition commonly used in the literature, namely a vanishing normal derivatives of the superconducting order parameter at the surface. The order parameter does not change until  $H = H_1$ . As  $H$  exceeds  $H_1$ , some quasi-particle energies are pushed below zero in Eq. (20) and contributions from these excited quasi-particle states reduce the order parameter in Eq. (14) by changing the signs of their contributions in the statistics factor,  $1 - 2f(E_{mj}^k)$ . In addition to an overall reduction of  $\Delta(\mathbf{r})$  under external field,  $\Delta(\mathbf{r})$  also changes slope, with a distinct knee that moves towards  $r = 0$  with increasing field (see arrows in Fig. 3). At a radius  $r$ , the angular momentum is of order  $m^*rv_F$  and the order parameter begins to be suppressed when  $\Delta \sim m^*v_F r H/2c$  or  $r \sim 2c\Delta/ev_F H$ . This simple argument should be taken with caution, since the semi-classical approximation of treating position and momentum as commutable in Eq. (14) becomes worse when there is a strong spa-

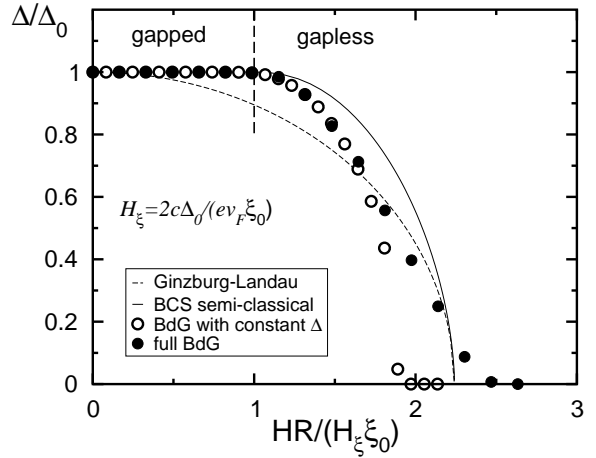


FIG. 1: Averaged superconducting order parameter in a cylindrical sample of large diameter ( $D = 200$  nm,  $D/\xi_0 = 0.57$ ) with axial external magnetic fields. Normalized order parameter to the zero field value  $\Delta/\Delta_0$  is plotted as a function of dimensionless field  $HR/(H_\xi \xi_0)$  with  $H_\xi = 2c\Delta_0/(ev_F \xi_0)$ . Overall agreement of the analytic formula Eq. (18) and the numerical results are good. Solution of Bogoliubov-de Gennes (BdG) equation in the clean limit remains constant until  $H_1 = 2c\Delta_0/ev_F R$ . Full solution of the BdG equation (solid circles) has larger order parameters near the critical field than those constrained to a spatially uniform  $\Delta$  (open circles) due

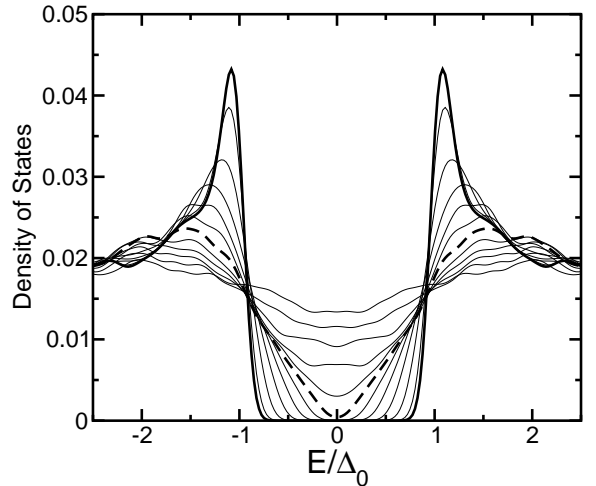


FIG. 2: Density of states as a function of external field. Superconductor becomes gapless at  $H = H_1$  (dashed line) in the clean limit well before the critical field  $H_c$ , due to the coupling of orbital angular momenta to external field. The external fields in the plot are from  $HR/(H_\xi \xi_0) = 0$  (thick line) to 1.83 with equal intervals between the curves.

tial variation.<sup>21</sup> At larger radius  $r$ , the energy difference between the angular momenta (with  $m\hbar \sim m^*rv_F$ ) in an electron pair exceeds the pairing energy and therefore the pair becomes depaired.

We emphasize that the pronounced radial dependence of order parameter is related to the coupling of orbital

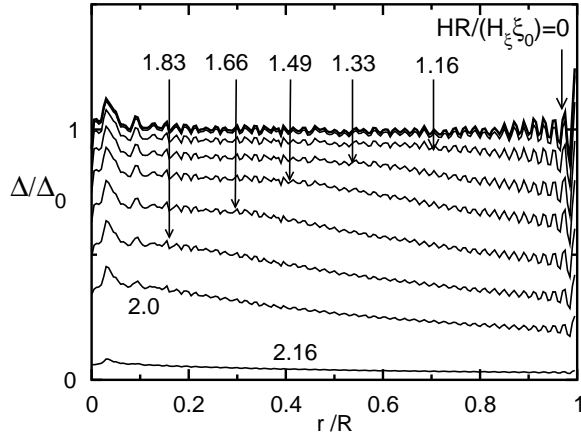


FIG. 3: Spatial variation of order parameter  $\Delta$  in the large diameter limit ( $D/\xi_0 = 0.57$ ). For external fields of  $0 < H < H_1$ ,  $\Delta$  remains flat. As the field increases from  $H_1$ ,  $\Delta$  drops with a knee which progresses towards  $\mathbf{r} = 0$ .

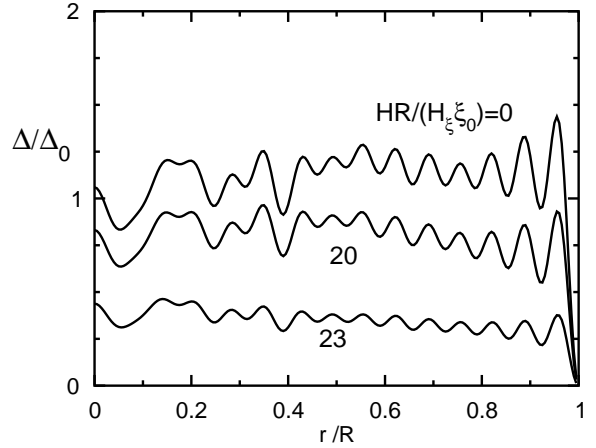


FIG. 4: The order parameter  $\Delta$  as a function of the radius at small diameter  $D/\xi_0 = 0.057$  ( $\delta R = 2 \text{ \AA}$ ). The spatial variation of  $\Delta$  is much stronger than for the large diameter wires of Fig. 3.

## B. Small diameters

angular momentum to the external field, rather than the term  $\frac{1}{8}m^*\omega_c^2r^2$  in Eq. (5), which makes the superconducting order parameter more massive. To compare these two contributions, we consider the Ginzburg-Landau theory with an order parameter of zero total angular momentum, as is usual in the literature<sup>7,8</sup>; (see appendix B). The order parameter couples to the external field only through  $\frac{1}{8}m^*\omega_c^2r^2$  and does not have any information about the angular momenta of constituent electrons in Cooper pairs. The spatial dependence of  $\Delta(r)$  arising from the term  $(2e/\hbar c)^2\mathbf{A}^2$  turns out to be much weaker than the angular momentum coupling in the BdG treatment. The resulting critical field Eq. (B5) is almost identical to the angular momentum depairing result Eq. (19), as both are derived in detail in the appendix.

It is interesting to note that, although the orbital coupling and the  $A^2$ -coupling produce very close critical fields (see Eqs. (19,B5)) in the absence of the other, they do not act additively when both are present. When the  $A^2$ -term is included on top of the orbital coupling, its effect becomes significantly smaller than in Eq. (B5) because the orbital effect produces fast-decaying  $|\Delta(r)|^2$  near  $H = H_c$ . For example, the curve labeled with  $HR/(H\xi_0) = 2.16$  in Fig. 3 has  $|\Delta(r = R)|^2/|\Delta(r = 0)|^2 \approx 1/7$ . Since the  $A^2 \sim H^2r^2$  term couples most strongly at large  $r$ , the actual  $A(r)^2|\psi(r)|^2$  coupling is much smaller than the Ginzburg-Landau theory. For instance, a reduction of the effective  $A^2$ -coupling by half results in the reduction of the order parameter by  $\sqrt{1/(1+0.5)} \approx 82\%$  in terms of the Ginzburg-Landau theory when the both couplings are naively added, which nearly matches the discrepancy in Fig. 1 between the Eq. (18) (thin line) and the constant- $\Delta$  (open circles) results.

When the diameter shrinks sufficiently that the transverse level spacings  $\delta E$  exceed the order parameter  $\Delta$ , the density of states on the energy scale of  $\Delta$  becomes spiky and spatial structure arising from the transverse modes begins to show up in the radial dependence of  $\Delta(\mathbf{r})$ . Since the level spacing of the transverse modes is inversely proportional to the effective mass ( $\delta E = \hbar^2/m^*R^2$ ), the effect of the discrete levels will be strong for systems of small effective mass or low transition temperature. Fig. 4 shows the spatial variation of the order parameter in this regime. A close examination reveals two characteristic length scales in  $\Delta(\mathbf{r})$ . The shorter length scale (with rapid oscillations more apparent at large radius) is given in terms of the Fermi velocity, i.e.,  $\Delta r \sim 2\pi\hbar/m^*v_F$ . As the Fermi velocity (or the carrier density) grows,  $\Delta(\mathbf{r})$  oscillates more rapidly.

Apart from the structures corresponding to the Fermi wavelength, there are more interesting and slowly varying spatial modulations, particularly near  $r = 0$ . Although these modulations also appear for large diameters (see Fig. 3), their relative importance grows in the smaller diameter wires. This spatial structure arises from the small number of transverse modes within the energy window  $[-\omega_D, \omega_D]$ . As can be seen from Eqs. (14, A3), the energy levels close to the Fermi energy contribute strongly to the order parameter  $\Delta$ . Since the density of states is peaked at the transverse energy levels (see Eq. 16), the resulting order parameter has larger amplitude for the states with  $\hbar^2\alpha_{mj}^2/2m^*R^2 \approx \mu$ ,  $k_z \approx 0$  and displays the spatial characteristics of those transverse modes. As illustrated in Fig. 5, the states within the  $k$ -space shell of area  $2\pi k_F \delta k_\perp \sim 4\pi m^*\omega_D$  contribute most strongly to the order parameter. Although we have used sharp energy cut-offs at  $\omega_D$ , they are not expected to impose a significant quantitative change because the weight factor in

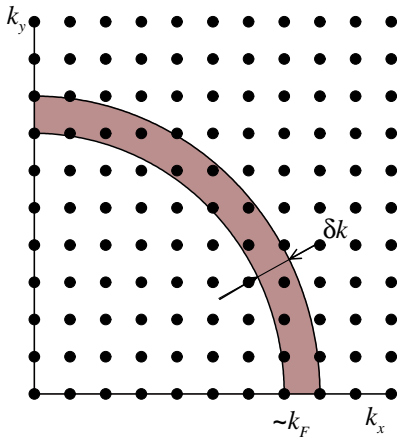


FIG. 5: Schematic 2-dimensional phase space with zero z-axial wavevector ( $k_z = 0$ ). Transverse modes within the shell of thickness  $\delta k_{\perp}$  contribute strongly to the order parameter. The area of the shell  $2\pi k_F \delta k_{\perp} \sim 4\pi m^* \omega_D$  does not depend on the choice of Fermi energy.

the gap equation,  $u_{\alpha}v_{\alpha} \approx \Delta/2\sqrt{\varepsilon_{\alpha}^2 + \Delta^2}$  (cf. Eq. (A2)), is small near the cutoff. The ratio of  $u_{\alpha}v_{\alpha}$  for  $\varepsilon_{\alpha} = 0$  to  $\varepsilon_{\alpha} = \omega_D$  is approximately  $\omega_D/\Delta \approx 25$ .

The shape of the order parameter is determined by which states happen to fall into the  $k$ -space shell. For instance, if states of ( $m = 0$ ) are absent in the shell, then the amplitude  $\Delta(\mathbf{r} \simeq 0)$  is depleted, since only the Bessel functions of  $J_{0j}$  have non-vanishing values at  $r = 0$ . We caution that the order parameter is not necessarily zero at  $r = 0$ , since there are also states ( $mjk$ ) with finite  $k$ . As the diameter decreases, the transverse states become more sparse in the energy shell and the spatial structure becomes more pronounced. In contrast, large-diameter wires have many contributing ( $mj, k = 0$ ) states and the spatial variation averages out.

Averaged order parameters  $\Delta$  at zero magnetic field are plotted as a function of diameter in Fig. 6. The temperature is fixed at 0.2 K and 3 different radial smearings  $\delta R = 0, 2, 5 \text{ \AA}$  are used. The filled circles are solutions for full BdG equations and the open circles impose the constraint of a constant  $\Delta$ . Regardless of  $\delta R$  and the spatial constraint,  $\Delta/\Delta_0$  converges to 1 at large diameter.  $\Delta$  fluctuates considerably as the diameter decreases, with more scatter for smaller radius smearing. These variations arise from the sharp van Hove singularities in the density of states at transverse eigenvalues. Interestingly, the full BdG order parameter is consistently larger than the constant  $\Delta$  solution. The gap equation, Eq. (14) or (A3), becomes particularly simple for a constant  $\Delta$  at  $T = 0$ ,

$$\frac{1}{V} = \int_0^{\omega_D} \frac{\rho_D(\omega) d\omega}{\sqrt{\omega^2 + \Delta^2}}, \text{ with } \rho_D(\omega) = \sum_{\alpha} \delta(\varepsilon_{\alpha} - \omega), \quad (21)$$

where  $\varepsilon_{\alpha}$  is the non-interacting eigenvalue (absorbing chemical potential). Although the density of states  $\rho_D(\omega)$  at diameter  $D$  has fluctuations due to discrete

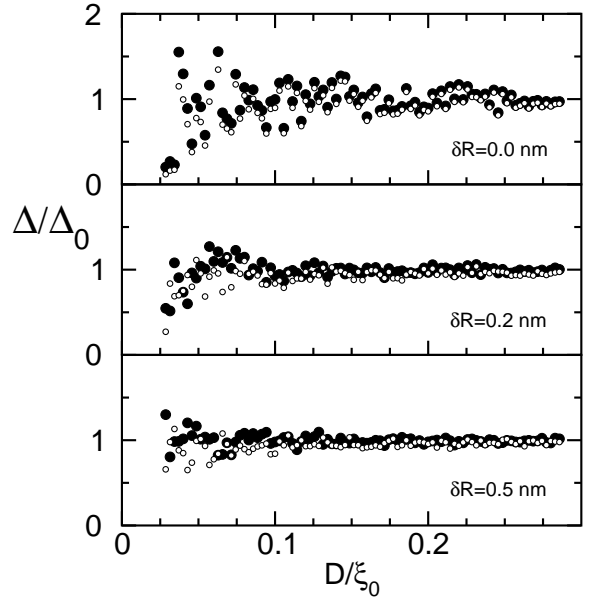


FIG. 6: Average order parameters  $\Delta$  as a function of diameter for different radius smearings  $\delta R$ . Filled circles are the full BdG solution while empty circles represent the constrained case where spatial variation of  $\Delta$  is disallowed. Confinement effects appear at  $D/\xi_0 \sim 0.1$ , i.e., when the transverse energy level spacing  $\delta E \approx \Delta$ .  $\Delta$  converges to about 4 K as the diameter increases, regardless of  $\delta R$ . In the full solution,  $\Delta$  increases slightly as  $D/\xi_0$  drops below about 0.1. Compared to the constant- $\Delta$  behavior, this enhanced order parameter takes advantage of the spatial variation in the BdG solution.

transverse energy levels, it averages to the bulk limit. Therefore, statistically,  $\Delta$  is expected to fluctuate about the bulk value  $\Delta_0$ . Particular lineshape of the curves (of empty circles) in Fig. 6 is due to limited diameter sampling and the fine-tuning of model parameters. As the calculation of  $\delta R = 0.5 \text{ nm}$  indicates, stronger broadening suppresses the fluctuation of the order parameter which will converge to  $\Delta_0$  down to small  $D$ . When the condition of the uniform  $\Delta$  is relaxed, the  $\Delta$  has the freedom to peak in regions with a higher density of electronic states, thereby increasing the condensation energy. For all  $\delta R$  shown here, the enhanced order parameter is most evident for  $D/\xi_0$  smaller than about 0.1, the diameter regime where the transverse level spacing becomes comparable to  $\Delta$ . For  $D/\xi_0$  of 0.05-0.1, the enhancement is roughly 10–20 %. This is consistent with larger  $T_c$  in small samples, as is often observed in thin films<sup>23,24,25</sup>. This tendency has been attributed to softening of surface phonons in samples of small dimension. The spatial variation of the order parameter  $\Delta$  from confinement effects may also contribute to this trend.

The order parameter  $\Delta$  versus magnetic field plotted in Fig. 7 shows shoulders that also reflect the discrete nature of the transverse modes. The overall shape of the curves is similar to that for large diameters (see Fig. 1).  $\Delta$  remains constant until the depairing field  $e_h$

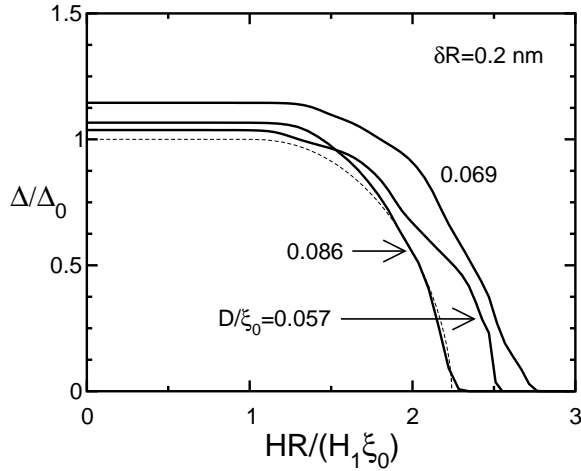


FIG. 7: The order parameter  $\Delta$  as a function of the external field at a small diameter  $D/\xi_0 = 0.057 - 0.086$  ( $D = 20 - 30$  nm,  $\delta R = 2$  Å).  $\Delta$  displays several shoulders as the field increases and then vanishes abruptly, unlike the large diameter case of Fig. 1. This structure reflects the discrete nature of the transverse modes. The sudden cut-off of  $\Delta$  at the critical field is due to an absence of small angular momentum transverse states near the chemical potential. The dashed line is Eq. (18).

in Eq. (A3) becomes comparable to  $\Delta$ . As the field increases further, distinctive shoulders appear. As shown in Eq. (A3), until the condition  $\sqrt{\varepsilon_\alpha^2 + \Delta^2} < e_{h\alpha}$  is satisfied for any non-interacting state  $\alpha$ , the thermal factor  $1 - 2f$  does not change, so the gap equation yields the same  $\Delta$ . At large diameters, the number of depaired states with  $\sqrt{\varepsilon_\alpha^2 + \Delta^2} > e_{h\alpha}$  increases gradually and  $\Delta$  therefore varies steadily with the external field  $\mathbf{H}$ . However, at small diameters, the density of states has peaked structures with van Hove singularities separated by an energy spacing of  $\hbar^2/m^*R^2$ . Since only a few transverse energy peaks are available in the energy window, the van Hove singularities have a stronger influence on the order parameter. Therefore kinks begin to appear in the field dependence of  $\Delta$ . As  $D$  grows, these discrete structures smooth out, as in Fig. 1.

The  $R$ -dependence of the critical field  $H_c$  is shown in Fig. 8. Electron orbits in more tightly confined spaces are less influenced by magnetic field, because of the smaller depairing contribution  $(e/\hbar c) \int d\ell \cdot \mathbf{A}$  in the phase of wavefunction. The filled circles are BdG solutions with  $\delta R = 2$  Å and the dashed line is the semi-classical (*i.e.*  $1/R$ ) solution of the BCS equation Eq. (19). The inset magnifies the small diameter regime. The BdG solution follows the  $1/R$  trends well down to about  $D/\xi_0 \sim 0.02$ . As  $D$  gets smaller,  $H_c$  fluctuates substantially, but follows the overall  $1/R$  behavior surprisingly well. One of our finding is that the prediction of the Ginzburg-Landau theory agrees remarkably well with the microscopic solution of the BCS equation, down to small diameters ( $D \ll \xi_0$ ). This conclusion may change with an inclusion of strong interaction effects, such as increasing Coulomb

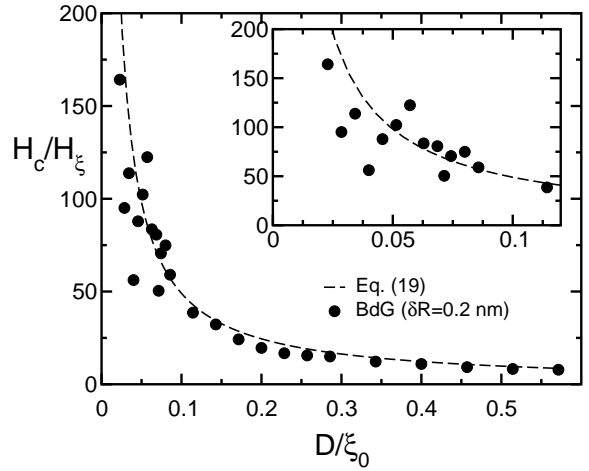


FIG. 8: The critical field vs rod diameter. The critical field  $H_c$  varies inversely proportional to the diameter  $D$ . The solutions of the full BdG equation follow the general trend of Eq. (19), which was obtained from the BCS equation under the constraint of a spatially constant order parameter. The full BdG solution satisfies the  $1/R$  prediction down to fairly small diameters, far smaller than coherence length, although they fluctuate strongly about the relation Eq. (19).

interaction in strong confinement at small diameters.

Finally, we mention that temperature dependence of the order parameter does not show significant deviation from the BCS results<sup>26</sup>. The relation  $\Delta/k_B T_c = 1.764$  holds to high accuracy for a wide range of diameters at zero external field.

#### IV. CONCLUSIONS

We have studied the dynamics of the transverse degrees of freedom in superconducting nanowires. As the confinement dimension shrinks and the level spacing becomes comparable to the order parameter  $\Delta$ , the discrete nature of the transverse modes shows up in a spatial variation of  $\Delta$ . In the clean limit, electronic angular momenta are conserved and couple strongly to magnetic field to shift the quasi-particle energy levels. This effect shows up as distinct shoulders in the response to an external field. In a confinement scale comparable to or larger than the superconducting coherence length, superconducting wavefunctions satisfy the usual boundary condition for normal derivative  $\partial\psi/\partial\mathbf{n} = 0$  for superconducting order parameter  $\psi$ . Under zero magnetic field,  $\psi$  remains constant throughout the sample, except for small and rapid oscillations. With finite external field,  $\psi$  adjust to the vector potential with much stronger spatial variations than predicted in Ginzburg-Landau theory.

Our results are relevant to clean-limit samples with inclusion of level broadening effects introduced by uncertainties in diameter. It is useful to compare the results with the dirty-limit theories<sup>7,8,12,16</sup>. Although detailed mechanisms for both limits are different, both systems

display gapless behavior. The critical fields for the disappearance of order parameters,  $H_c$ , behave quite differently for the two limits. In the dirty limit<sup>12</sup> ( $\ell/\xi_0 \ll 1$ ),  $H_c$  becomes very large (before the spin-Zeeman depairing effect dominates<sup>20</sup>), with  $H_c(\ell) \sim H_c \sqrt{\xi_0/\ell} \gg H_c$  with  $H_c$  given in Eq. (19) for the clean limit ( $\ell/\xi_0 \gg 1$ ). For the critical field  $H_1$  where the excitation spectrum first becomes gapless,  $H_1/H_c|_{\ell=0} = 0.954$  while  $H_1/H_c|_{\ell=\infty} = 0.389$ . Therefore, the clean limit remains gapless for a wide part of the magnetic field range compared to only 4.6% of the dirty limit. While the on-set of the order parameter suppression and the disappearance of the excitation gap happen simultaneously in the clean limit, the closing of the excitation gap in the dirty limit happens only when the superconducting order is already suppressed significantly.

Electrodeposition into nanoporous membranes such as polycarbonate or anodic alumina<sup>13</sup> can yield single-crystal metallic nanowires from several different superconducting metals (tin, lead, etc.). Such systems may be able to access the clean limit in which the phase information of definite angular momentum states is conserved and orbital-derived level-shifts under magnetic field become substantial. Since the effects of discrete levels begin to appear when the level spacing becomes comparable to the order parameter  $\Delta$  (cf. Eq. (17)), systems of smaller  $\Delta$  will exhibit stronger confinement effects at a given wire diameter. Systems with small band mass  $m^*$  will have similarly strong confinement effects.

The nature of confined superconductivity in single-crystalline metallic nanorods could perhaps be verified most clearly by the gapless spectrum that appears at magnetic fields smaller than the critical field. The small quasi-particle excitation energy here could result in very interesting physics, *e.g.* in specific heat measurements at temperatures below  $T_c$  under external field. Gapless superconductivity under an external field could also enhance phase-slip rates as reflected in the electrical resistivity. Due to the low quasi-particle excitation energies, thermal or quantum fluctuations will overcome the condensation energy more easily. Gapless excitations for normal electrons could contribute to a finite residual resistance in the presence of strong scattering at the confining surface.

### Acknowledgments

We thank M. Tian, M. Chan and Y. Liu for very helpful discussions. We acknowledge support from the National Science Foundation DMR-0213623 and the David and Lucile Packard Foundation.

### APPENDIX A: SEMI-CLASSICAL SOLUTION FOR ORDER PARAMETER $\Delta$ IN CYLINDER

We derive the analytic solution to the gap equation Eq. (14) with the constraint of a uniform order parameter  $\Delta$ . The relevant regime is when the cylinder is large enough that the transverse level spacing is much smaller than  $\Delta$  and the external field is not too close to the critical value. Similar results have been derived for spherical systems using a Green function technique.<sup>12</sup> With the assumption of a constant  $\Delta$ , one approximates  $[\mathbf{r}, \mathbf{p}] \approx 0$ , treating  $\mathbf{r}$  and  $\mathbf{p}$  as independent variables. We ignore the Zeeman term from spins,  $\mu_B \boldsymbol{\sigma} \cdot \mathbf{H}$  in Eq. (2), since it is negligible in the regime of interest. The term quadratic in the field,  $e^2 \mathbf{A}^2 / 2m^*c^2$ , is also dropped, as discussed below. Under these conditions, the non-interacting Hamiltonian becomes  $H_0 = \varepsilon_{\mathbf{k}} - e_h$ , where  $\varepsilon_{\mathbf{k}} = \frac{1}{2}m^*v^2 - \mu$  and

$$e_h = \frac{e}{2m^*c} \mathbf{L} \cdot \mathbf{H}. \quad (\text{A1})$$

Solving the BdG equation Eq. (1) for a constant  $\Delta$ , one obtains

$$E_{\mathbf{k}} = \sqrt{\varepsilon_{\mathbf{k}}^2 + \Delta^2} - e_h, \text{ and } u_{\mathbf{k}} v_{\mathbf{k}} = \frac{\Delta}{2\sqrt{\varepsilon_{\mathbf{k}}^2 + \Delta^2}}. \quad (\text{A2})$$

With these approximations,  $u_{\mathbf{k}} v_{\mathbf{k}}$  is independent of the field  $\mathbf{H}$ . The gap equation can be written as

$$1 = V \sum_{\mathbf{k}} \frac{1 - 2f(\sqrt{\varepsilon_{\mathbf{k}}^2 + \Delta^2} - e_h)}{2\sqrt{\varepsilon_{\mathbf{k}}^2 + \Delta^2}}. \quad (\text{A3})$$

The effect of the magnetic field is reflected only in the Fermi-Dirac function  $f$ . To evaluate the angular momentum summation, we write  $e_h = (e/2m^*c) \mathbf{L} \cdot \mathbf{H} = (e/2c)(\mathbf{r} \times \mathbf{v}) \cdot \mathbf{H} = (e/2c)(\mathbf{H} \times \mathbf{r}) \cdot \mathbf{v}$ . Now, with a fixed  $\mathbf{r}$  and  $\mathbf{H}$  and an isotropic distribution of  $\mathbf{v}$ ,  $e_h = (ev_F/2c)RH \cos \varphi$  with the angle  $\varphi = \angle(\mathbf{H} \times \mathbf{r}, \mathbf{v})$  and  $|\mathbf{v}| \approx v_F$ . The summation on the right-hand side of the gap equation Eq. (A3) becomes

$$\int_{-\omega_D}^{\omega_D} d\varepsilon N_0 \int_0^R \frac{2\pi dr r}{\pi R^2} \int \frac{d\Omega_v}{4\pi} \frac{1 - 2f}{2\sqrt{\varepsilon^2 + \Delta^2}}, \quad (\text{A4})$$

where  $N_0$  is the density of states and  $\Omega_v$  the solid angle for  $\mathbf{v}$ . If  $e^2 \mathbf{A}^2 / 2m^*c^2$  is much smaller than the integral limit  $\omega_D$ , it can be absorbed in the chemical potential with little change in the integral  $\int d\varepsilon$ . The gap equation becomes

$$1 = N_0 V \int_0^{\omega_D} d\varepsilon \int_0^1 du u \int_{-1}^1 d\mu \frac{1 - 2f(\sqrt{\varepsilon^2 + \Delta^2} - h u \mu)}{\sqrt{\varepsilon^2 + \Delta^2}}, \quad (\text{A5})$$

with  $u = r/R$ ,  $\mu = \cos \varphi$  and  $h = (ev_F/2c)RH$ . For  $H = 0$ , we have

$$\begin{aligned} 1 &= N_0 V \int_0^{\omega_D} d\varepsilon \int_0^1 du u \int_{-1}^1 d\mu \frac{1 - 2f(\sqrt{\varepsilon^2 + \Delta_0^2})}{\sqrt{\varepsilon^2 + \Delta_0^2}} \\ &= N_0 V \ln \left( \frac{\omega_D + \sqrt{\omega_D^2 + \Delta_0^2}}{\Delta_0} \right). \end{aligned} \quad (\text{A6})$$

Since  $f = 0$  for  $\sqrt{\varepsilon^2 + \Delta^2} > h\mu$  in the  $T = 0$  limit, we can perform the integral in Eq. (A5)

$$\begin{aligned} & \int_0^{\omega_D} d\varepsilon \int_0^1 du u \int_{-1}^1 d\mu \frac{f(\sqrt{\varepsilon^2 + \Delta^2} - h\mu)}{\sqrt{\varepsilon^2 + \Delta^2}} \\ &= \frac{1}{2} \left( 1 + \frac{1}{2\alpha^2} \right) \ln \left[ \alpha + \sqrt{\alpha^2 - 1} \right] - \frac{3}{4} \sqrt{1 - \alpha^{-2}}, \end{aligned}$$

for  $\alpha = h/\Delta > 1$ , and 0 for  $\alpha < 1$ . For  $\alpha > 1$ , Eq. (A5) becomes

$$\begin{aligned} 1 &= N_0 V \left\{ \ln \left( \frac{\omega_D + \sqrt{\omega_D^2 + \Delta^2}}{\Delta} \right) \right. \\ &\quad \left. - \left( 1 + \frac{1}{2\alpha^2} \right) \ln \left[ \alpha + \sqrt{\alpha^2 - 1} \right] + \frac{3}{2} \sqrt{1 - \alpha^{-2}} \right\}. \end{aligned} \quad (\text{A7})$$

Subtracting Eq. (A6) from Eq. (A7) and using  $\omega_D \gg \Delta_0$ , we obtain Eq. (18). The order parameter  $\Delta$  becomes gapless as one or both of the states in the time-reversed pairs in Eq. (A2) are pushed out of the Debye frequency. The external field influences  $T_c$  by the statistical factor, not directly through the field dependency in the non-interacting density of states, as can be inferred from Eq. (A5). The density of states over the interaction window of the Debye frequency remains nearly the same due to a balance between the outflux and the influx of non-interacting energy levels shifted by the external field.

## APPENDIX B: GINZBURG-LANDAU THEORY

Here we consider only a stationary superconducting order parameter ( $L_z = 0, k_z = 0$ ) where the Ginzburg-Landau functional for the order parameter  $\psi$  reads

$$F = -\alpha|\psi|^2 + \frac{\beta}{2}|\psi|^4 + \left| \left( \nabla - i\frac{2e}{\hbar c} \mathbf{A} \right) \psi \right|^2 \quad (\text{B1})$$

$$= \frac{H_c^2}{8\pi} \left[ -|f|^2 + \frac{|f|^4}{2} + \xi^2 \left| \left( \nabla - i\frac{m_0\omega_c r\hat{\theta}}{\hbar} \right) f \right|^2 \right]. \quad (\text{B2})$$

$H_c$  is the bulk critical field,  $\psi = \psi_0 f$  ( $|\psi_0|^2 = \alpha/\beta$ ),  $\omega_c = eH/m_0c$ ,  $m_0$  is free electron mass, and  $\xi$  is the coherence length. The Coulomb gauge is used for the vector potential  $\mathbf{A} = \frac{1}{2}rH\hat{\theta}$ . For radius  $R$  much smaller than the penetration depth, the screening of external fields is negligible, as assumed in the main text. With constant  $f$ , we obtain the average free energy after integration over the cylindrical nanowire,

$$F = \frac{H_c^2}{8\pi} \left[ \left( -1 + \frac{1}{2} \left( \frac{m_0\omega_c R\xi}{\hbar} \right)^2 \right) f^2 + \frac{1}{2} f^4 \right]. \quad (\text{B3})$$

We have also numerically minimized the free energy with a spatially varying  $f$ , but the spatial variation was far less significant (about 1 percent of the average order parameter for  $R/\xi = 0.5$ ) than that of the Bogoliubov-de Gennes results discussed in the text. Therefore, the following approximate value for the critical field is quite accurate. Minimizing Eq. (B3) over  $f$  gives

$$f = \left[ 1 - \frac{1}{2} \left( \frac{m_0\omega_c R\xi}{\hbar} \right)^2 \right]^{1/2}. \quad (\text{B4})$$

For vanishing  $f$ , the critical field is

$$H_c = \frac{\sqrt{2}}{\pi} \frac{\Phi_0}{\xi R} = 0.450 \frac{\Phi_0}{\xi R}, \quad (\text{B5})$$

with  $\Phi_0 = hc/2e$ .

---

<sup>1</sup> E. C. Stoner and E. P. Wohlfarth, Philos. Trans. R. Soc. London, Ser. A **240**, 599 (1948).  
<sup>2</sup> D. V. Averin and K. K. Likharev, J. Low Temp. Phys. **62**, 345 (1986).  
<sup>3</sup> “Molecular Electronics: Science and Technology”, eds. A. Aviram and M. Ratner, Annals of the New York Academy of Sciences **852**, New York (1998).  
<sup>4</sup> S. John, Phys. Rev. Lett. **58**, 2486 (1987); E. Yablonovitch, Phys. Rev. Lett. **58**, 2059 (1987).  
<sup>5</sup> J. M. Graybeal, P. M. Mankiewich, R. C. Dynes and M. R. Beasley, Phys. Rev. Lett. **59**, 2697 (1987).  
<sup>6</sup> D. C. Ralph, C. T. Black and M. Tinkham, Phys. Rev. Lett. **78**, 4087 (1997).  
<sup>7</sup> M. Tinkham, *Introduction to Superconductivity*, Krieger Publishing Company (1975).

<sup>8</sup> P. G. de Gennes, *Superconductivity of Metals and Alloys*, Addison-Wesley Publishing Company (1989).  
<sup>9</sup> H. Suderow, E. Bascones, A. Izquierdo, F. Guinea and S. Vieria, Phys. Rev. B **65**, 100519 (2002).  
<sup>10</sup> V. R. Misko, V. M. Fomin and J. T. Devreese, Phys. Rev. B **64**, 014517 (2001).  
<sup>11</sup> K. Maki, “Superconductivity” Vol. II, Chapter 18, R. D. Parks (ed.), Marcel Dekker, New York (1969).  
<sup>12</sup> S. Strässler and P. Wyder, Phys. Rev. **158**, 319 (1967).  
<sup>13</sup> M. Tian, J. Wang, J. Snyder, J. Kurtz, Y. Liu, P. Schiffer, T. E. Mallouk and M. H. W. Chan, *submitted to Appl. Phys. Lett.*  
<sup>14</sup> N. Giordano, Phys. Rev. B **41**, 6350 (1990).  
<sup>15</sup> A. Bezryadin, C. N. Lau and M. Tinkham, Nature **404**, 971 (2000).

<sup>16</sup> M. Kato and K. Maki, *J. Magn. Magn. Mater.* **226**, 280 (2001).

<sup>17</sup> Inclusion of finite angular momentum ( $L_z = \pm \hbar$ ) components in the BdG equation produced far smaller amplitudes than the zero angular momentum component. See also Ref.<sup>10</sup>.

<sup>18</sup> L. Larkin, *Zh. Eksperim. i Teor. Fiz.* **48**, 232 (1965) [English transl.: *Soviet Phys.-JETP* **21**, 153 (1965)].

<sup>19</sup> Eq. (19) gives a steeper drop of  $\Delta$  as  $h_c - h \approx -(\Delta^2/2h_c) \ln(h_c/\Delta)$  than typical  $\Delta/\Delta_0 = \sqrt{1 - h^2/h_c^2}$  ( $h_c = 2.24\Delta_0$ ).

<sup>20</sup> P. Fulde, *Adv. Phys.* **22**, 667 (1973).

<sup>21</sup> If the commutation relation between position and momentum is ignored,<sup>12,18</sup> we always have  $\Delta(\mathbf{r} = 0) = \Delta_0$  at arbitrary field since the vector potential is zero.

<sup>22</sup> For the curve of  $HR/(H\xi_0) = 2.16$  in Fig. 3,  $|\Delta(r)|^2$  decays nearly by a factor of 7 at  $r = R$ .

<sup>23</sup> M. Strongin, O. F. Kammerer, J. E. Crow, R. D. Parks, D. H. Douglass Jr. and M. A. Jensen, *Phys. Rev. Lett.* **21**, 1320 (1968).

<sup>24</sup> J. M. Dickey and A. Paskin, *Phys. Rev. Lett.* **21**, 1441 (1968).

<sup>25</sup> H. M. Jaeger, D. B. Haviland, B. G. Orr and A. M. Goldman, *Phys. Rev. B* **40**, 182 (1989).

<sup>26</sup> J. Bardeen, *Rev. Mod. Phys.* **34**, 667 (1962).